

Optimal design of nanoporous materials for electrochemical devices

Xuan Zhang¹ and Daniel M. Tartakovsky^{2,a)}

¹Department of Mechanical and Aerospace Engineering, University of California, San Diego, 9500 Gilman Drive, La Jolla, California 92093, USA

²Department of Energy Resources Engineering, Stanford University, 367 Panama Street, Stanford, California 94305, USA

(Received 29 December 2016; accepted 15 March 2017; published online 4 April 2017)

Unique macroscopic properties of nanoporous metamaterials stem from their microscopic structure. Optimal design of such materials is facilitated by mapping a material's pore-network topology onto its macroscopic characteristics. This is in contrast to both trial-and-error experimental design and design based on empirical relations between macroscopic properties, such as the often-used Bruggeman formula that relates a material's effective diffusion coefficient to its porosity. We use homogenization to construct such a map in the context of materials design that maximizes energy/power density performance in electrochemical devices. For example, effective diffusion coefficients and specific surface area, key macroscopic characteristics of ion transport in a hierarchical nanoporous material, are expressed in terms of the material's pore structure and, equally important, ion concentrations in the electrolyte and externally applied electric potential. Using these microscopic characteristics as decision variables, we optimize the macroscopic properties for two two-dimensional material-assembly templates and several operating conditions. The latter affect the material's performance through formation of an electrical double layer at the fluid-solid interfaces, which restricts the pore space available for ion transport. *Published by AIP Publishing.* [<http://dx.doi.org/10.1063/1.4979466>]

Advances in materials science offer a plethora of alternative strategies for generation of nanoporous metamaterials with prescribed pore structures.^{1,2} This opens the possibility of bottom-up design of application-specific materials that optimize a desired macroscopic property, e.g., permittivity¹ or electric capacitance.² When not done by trial-and-error, metamaterial assembly is often guided by phenomenological relations between macroscopic properties. For example, the effective diffusion coefficient, D^{eff} , for a material with porosity ω and tortuosity τ is estimated from the corresponding molecular diffusion in free solvent, D_m , by using an empirical model $D^{\text{eff}} = \omega D_m / \tau$; if supplemented with another assumption, $\tau = 1/\sqrt{\omega}$, this gives Bruggeman's relation $D^{\text{eff}} = \omega^{3/2} D_m$.

Reliance on such macroscopic relations has a number of limitations. They provide insufficient information about the pore structure and, hence, are of limited use in its design. Moreover, their veracity is questionable, especially when (in the case of diffusion) pores are small and concentration gradients are large. While Bruggeman's relation is widely used to model ion diffusion in charged porous media (e.g., Ref. 3 and references therein), it neglects the diffusion coefficient's reduction due to formation of an electrical double layer (EDL) on the electrolyte-solid interfaces. Effects of the latter phenomenon are magnified in nanoporous materials, wherein adjacent EDLs can overlap, appreciably restricting the pore space available for ion transport. Such materials are mooted as a breakthrough technology for energy storage.^{4,5}

Dynamic maps expressing macroscopic parameters in terms of microscopic properties of porous media are derived by means of upscaling techniques. Crucially, such parameters

depend not only on the pore structure but also on pore-scale processes that, in the case of electrochemical systems, affect the EDL formation. Examples of upscaling analyses of pore-scale electrochemical phenomena described by Poisson-Nernst-Planck's equations can be found in Refs. 6–11. Our goal is to use the results of one such analysis¹¹ to inform the design of hierarchical nanoporous materials, which optimizes a material's macroscopic properties (diffusion coefficient and electric capacitance) by using the pore structure and operation conditions (electrolyte concentration and externally imposed electric potential) as decision variables.

Macroscopic representations of a charged nanoporous material Ω treat it as a continuum, without separating it into the pore space \mathcal{P} and the solid skeleton \mathcal{S} . Macroscopic state variables, ion concentration in an electrolyte $C(\mathbf{x}, t)$, and the corresponding electric potential $\Phi(\mathbf{x}, t)$ are defined at every point $\mathbf{x} \in \Omega$ for time $t \geq 0$. For binary electrolytes, their spatial variability induces the macroscopic Nernst-Planck fluxes of anions (–) and cations (+), $\mathbf{J}_{\text{NP}}^{\pm} = -\nu_{\pm} \mathbf{D}^{\pm} (\nabla C + z_{\pm} C \nabla \Phi)$. Here, ν_{\pm} and z_{\pm} are the ions' dissociation coefficients and charges (valencies), respectively; F is the Faraday constant; R is the gas constant; T is temperature; $\hat{\Phi} = F\Phi/(RT)$; and \mathbf{D}^{\pm} are the effective diffusion coefficients. Accounting for charge neutrality ($z_+ \nu_+ + z_- \nu_- = 0$) and considering symmetric binary electrolytes ($\nu_+ = \nu_- \equiv \nu$ and $z_+ = -z_- \equiv z$) to simplify the presentation, the latter are second-order semi-positive-definite tensors given by¹¹

$$\mathbf{D}^{\pm} = \frac{D_m^{\pm} \omega}{G_{\pm}} \int_{\mathcal{P}_d} e^{\mp z \hat{\Phi}_{\text{EDL}}} (\mathbf{I} + \nabla_{\mathbf{y}} \chi_{\pm}^{\top}) d\mathbf{y}, \quad (1)$$

where ω is the material's porosity; D_m^{\pm} are molecular diffusion coefficients of cations and anions in the free electrolyte;

^{a)}tartakovsky@stanford.edu

$$G_{\pm} = \int_{\mathcal{P}_U} e^{\mp \hat{\varphi}_{\text{EDL}}} d\mathbf{y}, \quad \hat{\varphi}_{\text{EDL}} = \frac{F\varphi_{\text{EDL}}}{RT}, \quad (2)$$

\mathbf{I} is the identity matrix and $\varphi_{\text{EDL}}(\mathbf{y})$ is the electrical potential distribution inside the EDL, which satisfies a Poisson-Boltzmann equation (PBE),

$$\lambda_D^2 \nabla^2 \hat{\varphi}_{\text{EDL}} = \sinh(-z\hat{\varphi}_{\text{EDL}}), \quad \mathbf{y} \in \mathcal{P}_U, \quad (3)$$

subject to the boundary condition $\varphi_{\text{EDL}} = \varphi_{\Gamma}$ on the fluid-solid interface Γ_U . The \mathcal{U} -periodic vector functions $\boldsymbol{\chi}_{\pm}(\mathbf{y})$, which serve as a bridge between the pore scale and continuum scale by representing the pore-scale fluctuations of the EDL in the effective model of ion diffusion, are computed as solutions of boundary-value problems

$$\nabla_{\mathbf{y}} \left[e^{\mp z\hat{\varphi}_{\text{EDL}}} (\mathbf{I} + \nabla_{\mathbf{y}} \boldsymbol{\chi}_{\pm}^{\top}) \right] = 0, \quad \mathbf{y} \in \mathcal{P}_U \quad (4a)$$

subject to

$$\mathbf{n}(\mathbf{I} + \nabla_{\mathbf{y}} \boldsymbol{\chi}_{\pm}^{\top}) = 0, \quad \mathbf{y} \in \Gamma_U; \quad \int_{\mathcal{P}_U} \boldsymbol{\chi}_{\pm} d\mathbf{y} = 0. \quad (4b)$$

These are defined inside the pore space \mathcal{P}_U of the unit cell \mathcal{U} that serves as a building (periodically repeating) block of the nanoporous material Ω (e.g., those in Fig. 1). In (3), $\lambda_D^2 = (RT\mathcal{E})/(2F^2z\nu C_{\text{in}})$ is the square of the Debye length, with \mathcal{E} and C_{in} denoting the dielectric constant of the electrolyte and the initial ion concentration, respectively.

Tensorial nature of the effective diffusion coefficients stems from the material's pore structure, \mathcal{P}_U ; the latter directly affects the magnitude of $\boldsymbol{\chi}_{\pm}$ and, hence, \mathbf{D}^{\pm} . It follows from (1)–(4) that the off-diagonal components of the diffusion tensors \mathbf{D}^{\pm} are zero, $D_{ij}^{\pm} = 0$ for $i \neq j$. The diagonal terms are presented in the form of normalized binary diffusion coefficients,³

$$D_i \equiv \frac{2D_{ii}^+ D_{ii}^-}{D_{ii}^+ + D_{ii}^-}, \quad i = 1, 2, \quad (5)$$

which are normalized with D_m for $D_m^+ = D_m^- \equiv D_m$.

Equations (1)–(4) map the pore structure on the macroscopic material's property \mathbf{D}^{\pm} . The material's operational conditions affect these diffusion coefficients through the dependence of φ_{EDL} on the total (initial) ion concentration C_{in} and externally applied electric potential V . Alternative templates used to generate two-dimensional hierarchical nanoporous materials (Materials 1 and 2) are shown in Fig. 1.

We use sizes of the micropores and mesopores representative of materials proposed for electrical double layer capacitors.^{13,14} Specifically, the diameter of nanobridges (micropores) in Fig. 1 is set to $d = 0.7$ nm and their length to $l = 3$ nm; the mesopore radius R is allowed to vary between 2 nm to 5 nm; and the half-width of the throats between two adjacent mesopores is set to $r = 0.4$ nm.

The reliance on the PBE (3) to compute the EDL potential φ_{EDL} restricts our analysis to dilute concentrations. For example, the PBE was shown to yield accurate predictions for low concentrations of monovalent electrolytes.^{15,16} We use $C_{\text{in}} = 0.1$ M (mol/L) as the upper limit of ion concentration.

External voltage V is limited by the breakdown voltage of electrolyte species, V_{br} . For aqueous-solution electrolytes, V_{br} can reach 1.23 V, while for organic electrolytes V_{br} can be as high as 4 V.⁵ For a given V , the diffuse-layer potential, φ_{Γ} , on the charged material is estimated from

$$\varphi_{\Gamma} = \frac{V}{2} - \phi_{\text{ecm}} - \frac{\sigma}{C_H}, \quad (6)$$

where $\phi_{\text{ecm}} \sim 0.1$ – 0.25 V is electrical capillary maximum, $\sigma = \sigma(\varphi_{\Gamma})$ is the surface charge density, and $C_H \sim 20$ – 45 $\mu\text{F}/\text{cm}^2$ is the Helmholtz capacitance.^{11,16} For aqueous-solution electrolytes, this equation yields φ_{Γ} in the range between 0.2 V and 0.4 V. The results presented below are for $\varphi_{\Gamma} = 0.2$ and 0.4 V. Finite-element solutions of (3) and (4) and Gaussian quadratures in (1) and (2) are calculated with COMSOL software.

Prior to identification of pore structures that yield optimal macroscopic properties of Materials 1 and 2, we explore effects of the materials' operating regime (initial concentration C_{in} and diffuse-layer potential φ_{Γ}) on the principle components, D_1 and D_2 , of the normalized binary diffusion coefficient in (5). Figure 2 shows the dependence of D_1 and D_2 on mesopore radius R for fixed throat width $2r = 0.8$ nm, $\varphi_{\Gamma} = 0.2$ V and a range of values of C_{in} . Overall, Material 2 has larger effective diffusion coefficients D_1 and D_2 . The longitudinal diffusion coefficient of both materials, D_1 , exhibits qualitatively different behaviors for highly dilute ($C_{\text{in}} = 0.01$ M) and more concentrated ($C_{\text{in}} = 0.05$ and 0.1 M) electrolytes; $D_1 = D_1(R)$ is convex in the former case and concave in the latter. The highly dilute electrolyte has the EDL whose thickness exceeds that of its more concentrated counterparts; this reduces the pore space available for ion migration, resulting in diffusion coefficients D_1 which are smaller than those for uncharged materials.

The transverse diffusion coefficient, D_2 , for both materials generally decreases with mesopore radius R (Fig. 2). That is because the rise of R increases both porosity and, for the fixed

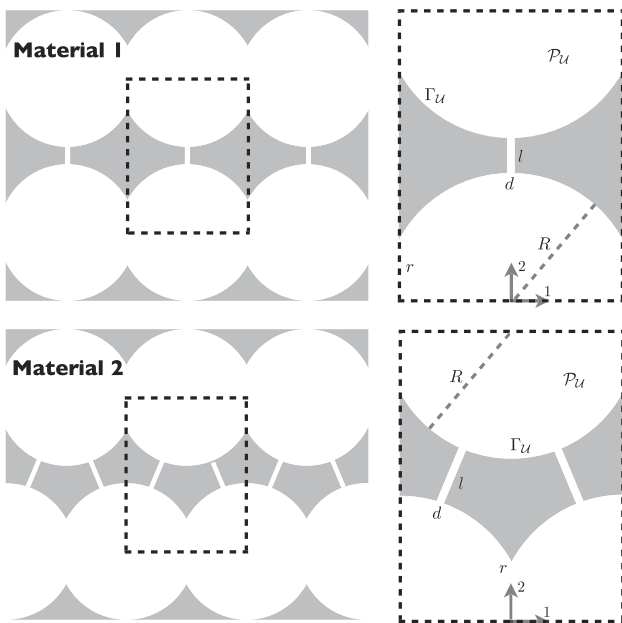


FIG. 1. Templates for generation of hierarchical nanoporous materials containing mesopores of radius R and micropores of diameter d (pore-throat size is $2r$).^{2,12}

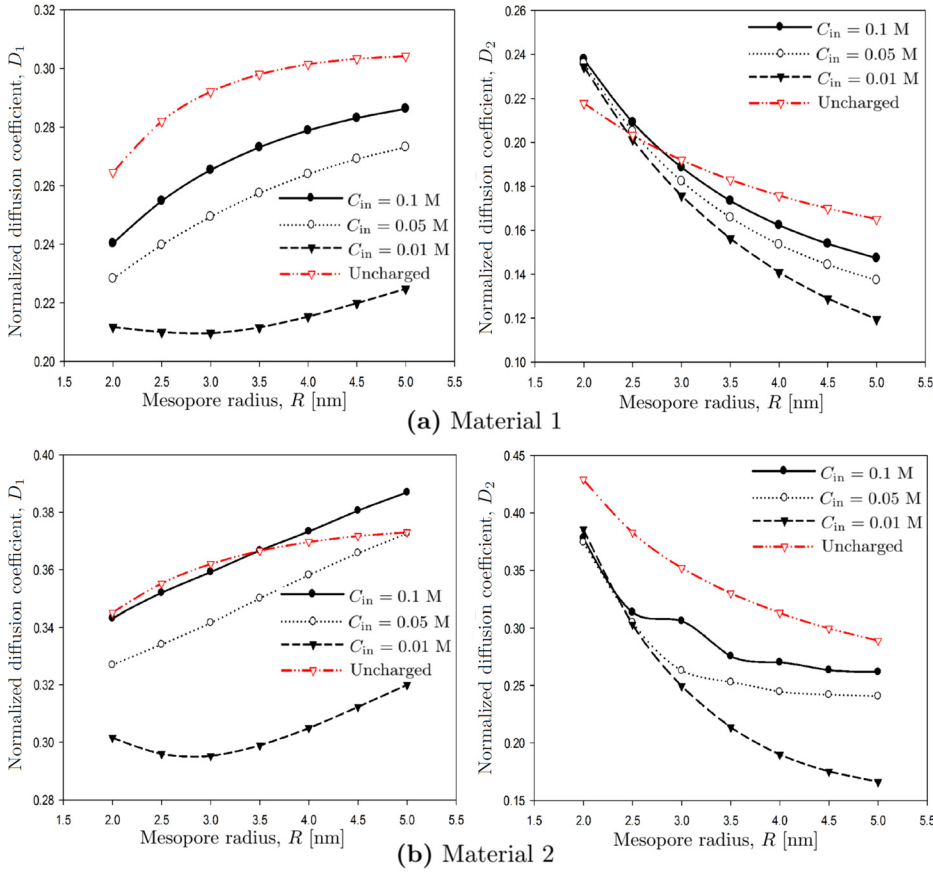


FIG. 2. Dependence of principal components, D_1 and D_2 , of the binary diffusion coefficient tensor on mesopore radius R , for Materials 1 and 2 with pore-throat width $2r = 0.8$ nm, diffuse-layer potential $\varphi_\Gamma = 0.2$ V, and several values of initial ion concentration C_{in} .

value of pore-throat width $2r$, tortuosity, with the latter having the dominant effect. The transverse diffusion coefficients D_2 for the electrically neutral Materials 1 and 2 for all R and C_{in} tend to exceed those for their electrically charged counterparts.

The non-monotonic behavior of $D_2(R)$ for Material 2 in Fig. 2 occurs at relatively low diffuse layer potential $\varphi_\Gamma = 0.2$ V and relatively high initial concentration $C_{in} = 0.1$ M. It might reflect the combined effects of externally applied voltage V , electrolyte concentration C_{in} , and pore structure. It vanishes when a larger electric field V is applied, resulting in $\varphi_\Gamma \geq 0.3$ M (Fig. 3).

The complex behavior of the effective diffusion coefficient for electrically charged materials, shown in Figs. 2 and 3, suggests a possibility of designing and fine-tuning nanoporous materials not only for specific applications but also for particular operating regimes. A material, which has optimal sorption characteristics under electrically neutral conditions,¹² might exhibit suboptimal electrosorption properties due to the presence of the EDL whose width is controlled by external conditions. Moreover, while mesopores provide good electrochemical accessibility but a relatively low specific surface area, micropores often have the size comparable to the Debye length and, hence, possess a large specific surface area but restrict ion transport. Hence, optimal design of such hierarchical nanoporous materials should involve optimization with respect to both the pore structure and operating conditions.

Suppose that our goal is to design a metamaterial that has both the maximum sorbing capacity (or, equivalently, specific surface area \mathcal{A}) and the binary diffusion coefficients that do not deviate by more than $\pm 5\%$ from their target values D_1^* and D_2^* ; the material is to operate in a device with

prescribed C_{in} and φ_Γ . This formulation gives rise to a constraint optimization problem

$$\max_{\mathbf{p} \in \mathcal{P}} \mathcal{A}(\mathbf{p}), \quad \mathbf{p} \equiv \{R, r, d, l\} \quad (7a)$$

subject to

$$0.95D_i^* \leq D_i(\mathbf{p}) \leq 1.05D_i^*, \quad i = 1, 2, \quad (7b)$$

where \mathcal{P} is the four-dimensional parallelepiped defining the low (L_{low}) and upper (L_{up}) limits of the four pore-scale decision variables $\{R, r, d, l\}$, whose values are reported in Table I. This table also contains the target values of the normalized binary diffusion coefficients D_1^* and D_2^* for Materials 1 and 2 that are estimated from their respective maxima in Fig. 3.

Solutions of the optimization problem (7) are obtained with the derivative-free Nelder-Mead method implemented in COMSOL. They are presented in Table II for operating conditions characterized by $\varphi_\Gamma = 0.3$ V and either $C_{in} = 0.1$ M or $C_{in} = 0.01$ M. For both material templates, optimal macroscopic properties are obtained by choosing the mesopore diameter $2R \sim 3-4$ nm, the mesopore-throat width $2r \approx 1.0$ nm, and the microchannels of diameter $d \approx 0.6$ nm and length $l \approx 3.3$ nm. In materials design, one should increase these values by adding the Stern layer's width. Both Materials 1 and 2 are nearly isotropic, with the longitudinal and transverse diffusion coefficients $D_1 \approx D_2$. Material 2 outperforms Material 1 in terms of both diffusive characteristics and electrosorption capacity (specific surface area).

In summary, charged solid materials exert considerable influence on the transport process via accumulation of ions within the EDL, affecting the optimal pore structure of nanoporous materials designed to handle, e.g., solute transport

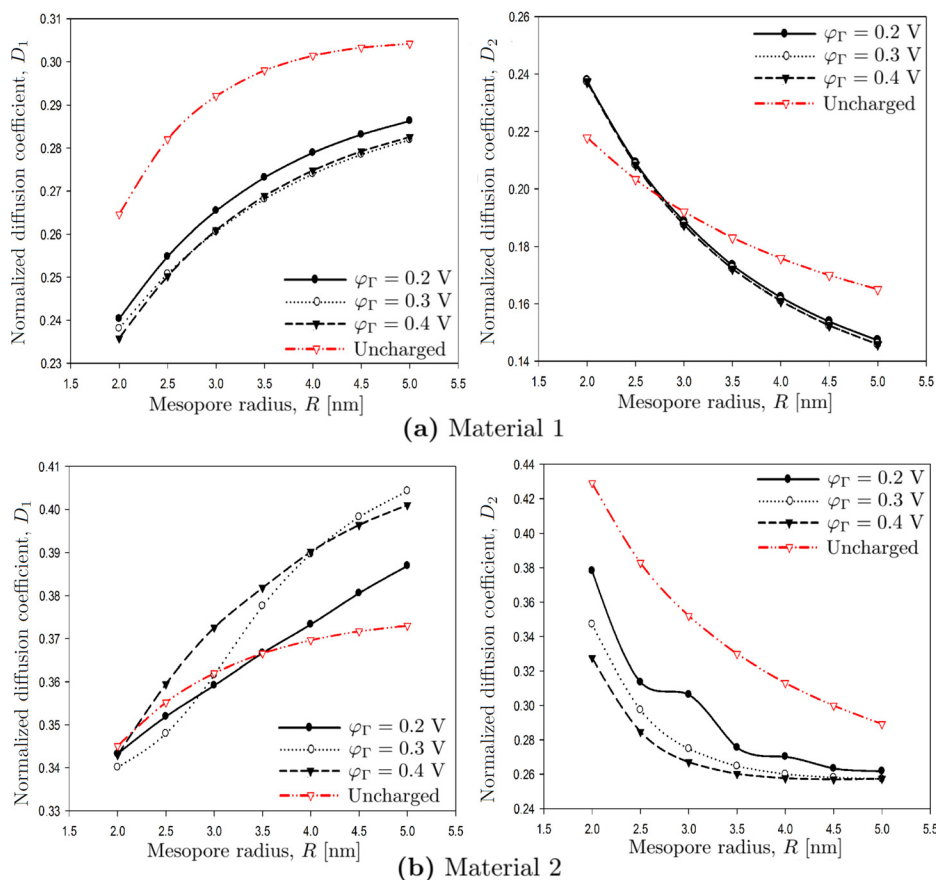


FIG. 3. Dependence of principal components, D_1 and D_2 , of the binary diffusion coefficient tensor on mesopore radius R , for Materials 1 and 2 with pore-throat width $2r=0.8$ nm, initial ion concentration $C_{in}=0.1$ M, and several values of diffuse-layer potential φ_{Γ} .

TABLE I. Low (L_{low}) and upper (L_{up}) limits of the pore-scale decision variables that define the pore structure of Materials 1 and 2. Target values for the longitudinal (D_1^*) and transverse (D_2^*) binary diffusion coefficients for these two materials.

	R (nm)	r (nm)	d (nm)	l (nm)
L_{low}	1.6	0.5	0.6	3.0
L_{up}	3.0	0.7	1.0	5.0
	Material 1		Material 2	
C_{in} (M)	D_1^*	D_2^*	D_1^*	D_2^*
0.01	0.24	0.24	0.37	0.37
0.1	0.24	0.23	0.36	0.36

TABLE II. Optimal microscopic and macroscopic properties of Materials 1 and 2.

C_{in} (M)	R (nm)	r (nm)	d (nm)	l (nm)	ω	D_1	D_2	\mathcal{A}
Material 1								
0.01	1.79	0.40	0.60	3.15	0.42	0.24	0.25	1.23
0.1	1.76	0.57	0.60	3.30	0.42	0.20	0.23	1.24
Material 2								
0.01	1.81	0.58	0.60	3.69	0.62	0.37	0.38	1.42
0.1	1.74	0.60	0.60	3.13	0.60	0.36	0.37	1.46

with Langmuir adsorption.¹² Optimal design of such materials is facilitated by mapping a material's pore-network topology onto its macroscopic characteristics. Homogenization theory was employed to construct such a map, which then was used to design materials with optimal energy/power density

performance. The latter step relied on two-dimensional material-assembly templates. Follow-up studies will deal with optimal selection from a set of three-dimensional templates.

This research was supported in part by the Defense Advanced Research Projects Agency under the EQUiPS program and the National Science Foundation under grant DMS-1522799.

- ¹J. Biener, G. W. Nyce, A. M. Hodge, M. M. Biener, A. V. Hamza, and S. A. Maier, *Adv. Mater.* **20**, 1211–1217 (2008).
- ²H. Yamada, H. Nakamura, F. Nakahara, I. Moriguchi, and T. Kudo, *J. Phys. Chem. C* **111**, 227 (2007).
- ³J. Newman and K. E. Thomas-Alyea, *Electrochemical Systems* (John Wiley & Sons, 2012).
- ⁴J. Chmiola, G. Yushin, Y. Gogotsi, C. Portet, P. Simon, and P.-L. Taberna, *Science* **313**, 1760 (2006).
- ⁵B. E. Conway, *Electrochemical Supercapacitors: Scientific Fundamentals and Technological Applications* (Springer, 2013).
- ⁶A. Gully, H. Liu, S. Srinivasan, A. K. Sethurajan, S. Schougaard, and B. Protas, *J. Electrochem. Soc.* **161**, E3066 (2014).
- ⁷H. Arunachalam, S. Onori, and I. Battiato, *J. Electrochem. Soc.* **162**, A1940 (2015).
- ⁸M. Schmuck and M. Z. Bazant, *SIAM J. Appl. Math.* **75**, 1369 (2015).
- ⁹K. Sharma, Y.-H. Kim, J. Gabitto, R. T. Mayes, S. Yiacoumi, H. Z. Bilheux, L. M. H. Walker, S. Dai, and C. Tsouris, *Langmuir* **31**, 1038 (2015).
- ¹⁰T. D. Le, C. Moyne, and M. A. Murad, *Adv. Water Resour.* **75**, 31 (2015).
- ¹¹X. Zhang and D. M. Tartakovsky, *J. Electrochem. Soc.* **164**, E53 (2017).
- ¹²X. Zhang, K. Urita, I. Moriguchi, and D. M. Tartakovsky, *J. Appl. Phys.* **117**, 244304 (2015).
- ¹³O. Barbieri, M. Hahn, A. Herzog, and R. Kötz, *Carbon* **43**, 1303 (2005).
- ¹⁴K. Xia, Q. Gao, J. Jiang, and J. Hu, *Carbon* **46**, 1718 (2008).
- ¹⁵L. Yeomans, S. E. Feller, E. Sánchez, and M. Lozada-Cassou, *J. Chem. Phys.* **98**, 1436 (1993).
- ¹⁶K.-L. Yang, T.-Y. Ying, S. Yiacoumi, C. Tsouris, and E. S. Vittoratos, *Langmuir* **17**, 1961 (2001).